Chapter 3

Protonation of the Biologically Relevant Cu^{II} μ-Thiolate Complex: Ligand Dissociation or Formation of a Protonated Cu^{I} Disulfide Species?

The proton-induced electron-transfer reaction of a Cu^{II} μ-thiolate complex to a Cu^{I} containing species has been investigated, both experimentally and computationally. The Cu^{II} μ-thiolate complex $[Cu^{II}_2(\mathbf{L^2{*}S})_2]^{2+}$ was isolated with the new pyridyl-containing ligand $\mathbf{L^2{*}SSL^2{*}}$, which has the ability to form both Cu^{II} thiolate and Cu^{I} disulfide complexes depending on the solvent. Both the Cu^{II} and the Cu^{I} complexes show reactivity upon addition of protons. The new multivalent tetranuclear complex $[Cu^{I}_2Cu^{II}_2(\mathbf{L^1{*}S})_2(CH_3CN)_6]^{4+}$ crystallized after addition of two equivalents of strong acid to a solution containing the μ-thiolate complex $[Cu^{II}_2(\mathbf{L^1{*}S})_2]^{2+}$ and was further analyzed in solution. Our studies show that upon addition of protons to the Cu^{II} thiolate compound the ligand dissociates from the copper centers, in contrast to an earlier report describing redox isomerization to a Cu^{I} disulfide species that is protonated at the pyridyl moieties. Computational studies of the protonated Cu^{II} μ-thiolate and Cu^{I} disulfide species with $\mathbf{L^1{*}SSL^1{*}}$ show that already upon addition of two equivalents of protons, ligand dissociation forming $[Cu^{I}(CH_3CN)_4]^{+}$ and protonated ligand is energetically favored over conversion to a protonated Cu^{I} disulfide complex.

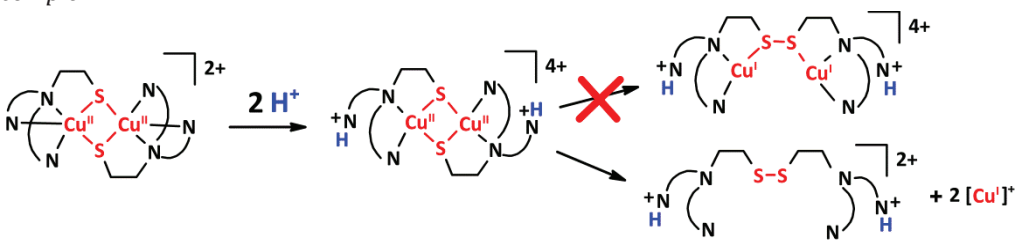

This chapter has been published as a full paper: E. C. M. Ording-Wenker, M. van der Plas, M. A. Siegler, C. Fonseca Guerra, E. Bouwman, *Chem. Eur. J.* **2014**, *20*, 16913-16921.

3.1 Introduction

The abundant occurrence of copper-sulfur redox chemistry in biological systems has attracted attention of inorganic chemists to study the equilibrium between Cu^{I} disulfide and Cu^{II} μ-thiolate species (Chapter 1). We found that upon addition of protons to a Cu^{II} μ-thiolate complex containing ligand **L¹*SSL¹***, a conversion takes place as indicated by a color change from dark green to light yellow. We decided to investigate this proton-induced conversion both with the ligand **L¹*SSL¹*** and a slightly modified analogue **L²*SSL²*** (Figure 3.1). The new ligand **L²*SSL²*** was synthesized, as it resembles the ligand **L²SSL²** for which we reported its solvent and temperature dependent Cu^{II} thiolate/Cu^{I} disulfide equilibrium when coordinated to copper (Chapter 2).[1]

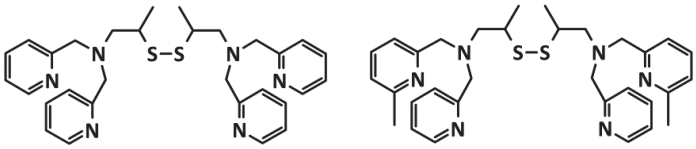

L¹*SSL¹* **L²*SSL²***

Figure 3.1: Schematic drawing of ligands **L¹*SSL¹*** and **L²*SSL²***.

Using protons to shift the redox equilibrium would provide an efficient way to trigger a copper-sulfur redox reaction in a controlled manner, giving new insights in proton-coupled electron transfer reactions in biological systems. During the course of our studies Stack and coworkers reported the dinuclear Cu^{II} μ-thiolate species with ligand **L¹*SSL¹*** upon addition of two equivalents of protons to convert to a Cu^{I} disulfide complex that is protonated at two of the pyridine groups (Section 1.4.4).[2] Addition of base was shown to reverse the reaction. Our studies, however, indicate that indeed the disulfide ligand is formed, but that it dissociates from the Cu^{I} centers already upon the addition of two equivalents of protons. DFT calculations were used to calculate the energies involved in this proton-induced conversion.

3.2 Results

3.2.1 Synthesis and Characterization of $[Cu^{I}_2Cu^{II}_2(\mathbf{L^{1*}S})_2(CH_3CN)_6](BF_4)_4$ and $[Cu^{II}_2(\mathbf{L^{2*}S})_2](BF_4)_2$

The ligands **L¹*SSL¹*** and **L²*SSL²*** were synthesized using a combination of reported procedures (Figure 3.2).[2-4]

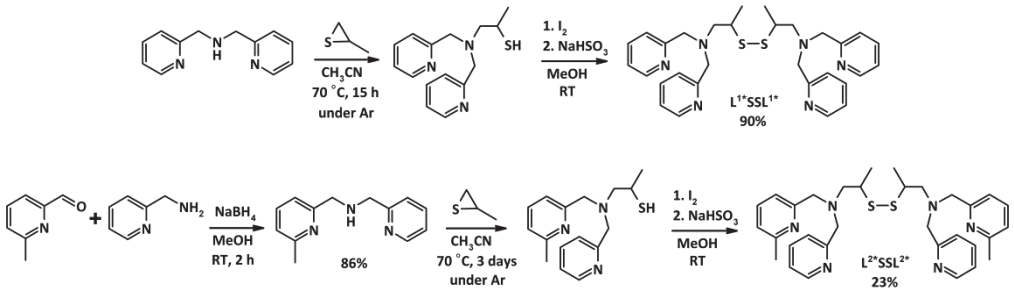

Figure 3.2: Schematic representation of the synthesis of **L¹*SSL¹*** and **L²*SSL²***.

Addition of 2 equivalents of $[Cu^{I}(CH_3CN)_4](BF_4)$ to **L¹*SSL¹*** dissolved in acetonitrile resulted in a dark green solution containing the Cu^{II} thiolate species $[Cu^{II}_2(\mathbf{L^{1*}S})_2]^{2+}$.[2] Subsequent addition of two equivalents of $HBF_4{\cdot}Et_2O$ resulted in a light brown solution to which diethyl ether was slowly added by vapor diffusion. This resulted in small black needle-like crystals of $[Cu^{I}_2Cu^{II}_2(\mathbf{L^{1*}S})_2(CH_3CN)_6](BF_4)_4$ as was unambiguously confirmed by X-ray structure determination. This complex can also be obtained by addition of 4 equivalents of $[Cu^{I}(CH_3CN)_4](BF_4)$ to **L¹*SSL¹*** dissolved in CH_3CN. When 2 equivalents of $[Cu^{I}(CH_3CN)_4](BF_4)$ were added to a solution of **L²*SSL²*** in acetone, again a dark green solution was obtained. Single crystals of the Cu^{II} μ-thiolate compound $[Cu^{II}_2(\mathbf{L^{2*}S})_2](BF_4)_2$ were obtained by vapor diffusion of pentane into this acetone solution; its structure was confirmed by single crystal X-ray crystallography. Projections of the cationic parts of the two structures are depicted in Figure 3.3.

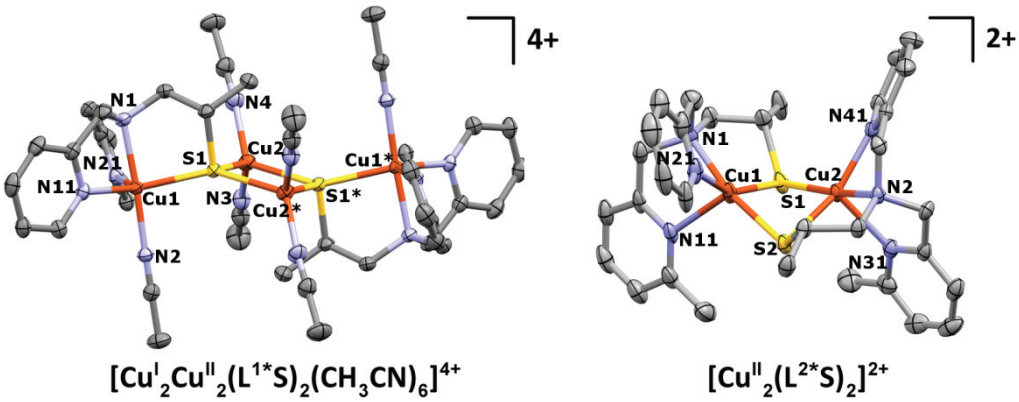

Figure 3.3: Displacement ellipsoid plots (50% probability level) of the cationic parts of $[Cu^{I}_2Cu^{II}_2(\mathbf{L^{1*}S})_2(CH_3CN)_6](BF_4)_4$ and $[Cu^{II}_2(\mathbf{L^{2*}S})_2](BF_4)_2$. Hydrogen atoms are omitted for clarity. Symmetry operation * = 1–x, 1–y, 2–z.

Table 3.1: Crystallographic and structure refinement data for complexes $[Cu^{I}_2Cu^{II}_2(\mathbf{L^{1*}S})_2(CH_3CN)_6](BF_4)_4$ and $[Cu^{II}_2(\mathbf{L^{2*}S})_2](BF_4)_2$.

	$[Cu^{I}_2Cu^{II}_2(\mathbf{L^{1*}S})_2(CH_3CN)_6](BF_4)_4$	$[Cu^{II}_2(\mathbf{L^{2*}S})_2](BF_4)_2$
empirical formula	$[C_{42}H_{54}Cu_4N_{12}S_2](BF_4)_4$	$[C_{32}H_{40}Cu_2N_6S_2](BF_4)_{1.8}(Cl)_{0.2}$
formula weight	1392.49	863.33
crystal system	monoclinic	monoclinic
space group	$P2_1/c$	$P2_1/n$
a, Å	12.2732(2)	10.3463(3)
b, Å	21.0952(2)	34.6731(11)
c, Å	12.1283(2)	11.4305(3)
β, deg	116.609(2)	99.087(2)
V, Å^3	2807.50(8)	4049.1(2)
Z	2	4
D_{calc}, g·cm^3	1.647	1.416
T, K	100(2)	110(2)
crystal size, mm	$0.40 \times 0.06 \times 0.05$	$0.44 \times 0.18 \times 0.03$
μ, mm^{-1}	3.266	2.938
no. of reflns measd	32508	25812
no. of unique reflns	5504	7877
no. of reflns obsd.	4993 [$I > 2\sigma(I)$]	6781 [$I > 2\sigma(I)$]
no. of parameters	457	632
R_1 / wR_2 [$I > 2\sigma(I)$]	0.0442/0.1216	0.0587/0.1657
R_1 / wR_2 [all refl.]	0.0478/0.1254	0.0669/0.1722
goodness of fit	1.084	1.076
$\Delta\rho$, e·Å^{-3}	−1.02 /0.78	−0.64 /0.96

Crystallographic data are provided in Table 3.1 and selected bond distances and angles are provided in Table 3.2 and Table 3.3.

The complex $[Cu^{I}_2Cu^{II}_2(\mathbf{L^{1*}S})_2(CH_3CN)_6](BF_4)_4$ crystallizes in the monoclinic space group $P2_1/c$ with one half of the tetranuclear complex cation and two tetrafluoridoborate anions per asymmetric unit; the tetranuclear complex is found at sites of inversion symmetry. Both BF_4^- counterions are disordered over two orientations; the occupancy factors of the major components of the disorder refine to 0.64(3) and 0.601(8). $[Cu^{I}_2Cu^{II}_2(\mathbf{L^{1*}S})_2(CH_3CN)_6](BF_4)_4$ is a tetranuclear mixed-valent complex containing two Cu^{I} and two Cu^{II} ions. The structure is best described as two Cu^{II} thiolate fragments $[Cu^{II}(\mathbf{L^{1*}S})(CH_3CN)]^+$ connected by two $[Cu^{I}(CH_3CN)_2]^+$ moieties, resulting in a planar four-membered Cu^{I}-S-Cu^{I}-S rhombus with Cu^{I}-S distances of 2.3102(7) Å and 2.4070(7) Å. The Cu^{II}-S distance is 2.3130(6) Å, which is similar to the Cu^{II}-S distances in the related Cu^{II} μ-thiolate structure $[Cu^{II}_2(\mathbf{L^{1*}S})_2]^{2+}$ (2.2909(8) Å and 2.3159(9) Å)[2] and in a similar multivalent complex $[Cu^{II}_4Cu^{I}_4(\mathbf{L^{1*}S})_4(\mu\text{-}OH)_2(CH_3CN)_6]^{6+}$ (2.34-2.36 Å) that is described in Chapter 4.[3]

Table 3.2: Selected bond distances and angles for $[Cu^{I}_2Cu^{II}_2(\mathbf{L^{1*}S})_2(CH_3CN)_6](BF_4)_4$.

Bond distance (Å)		Bond angle (°)	
Cu1 - Cu2	3.8679(5)	Cu1 - S1 - Cu2	113.57(3)
Cu1 - Cu2*	4.4799(5)	Cu1 - S1 - Cu2*	143.28(3)
Cu2 - Cu2*	3.4011(7)	Cu2 - S1 - Cu2*	92.25(2)
S1 - S1*	3.2703(11)	S1 - Cu1 - N1	88.10(6)
Cu1 - S1	2.3130(6)	S1 - Cu1 - N2	95.22(6)
Cu1 - N1	2.033(2)	S1 - Cu1 - N11	136.87(6)
Cu1 - N2	1.983(2)	S1 - Cu1 - N21	105.48(6)
Cu1 - N11	2.056(2)	N1 - Cu1 - N2	176.14(8)
Cu1 - N21	2.128(2)	N1 - Cu1 - N11	81.70(8)
Cu2 - S1	2.3102(7)	N1 - Cu1 - N21	82.61(8)
Cu2* - S1	2.4070(7)	N2 - Cu1 - N11	97.14(9)
Cu2 - N3	1.989(2)	N2 - Cu1 - N21	94.59(8)
Cu2 - N4	2.023(2)	N11 - Cu1 - N21	114.45(8)
		S1 - Cu2 - S1*	87.75(2)
		S1 - Cu2 - N3	132.02(7)
		S1 - Cu2 - N4	114.03(7)
		S1* - Cu2 - N3	105.86(7)
		S1* - Cu2 - N4	124.52(7)
		N3 - Cu2 - N4	95.82(10)

symmetry operation * = 1–x, 1–y, 2–z

The Cu^{II} ions are in an N_4S coordination environment, which can be best described as a highly distorted trigonal bipyramid ($\tau = 0.65$).[5]

$[Cu^{II}_2(\mathbf{L^{2*}S})_2](BF_4)_2$ crystallizes in the monoclinic space group $P2_1/n$. One BF_4^- counterion is found to be disordered over two orientations; the occupancy factor of the major component of the disorder refines to 0.510(6).

Table 3.3: Selected bond distances and angles for $[Cu^{II}_2(\mathbf{L^{2*}S})_2](BF_4)_2$.

Bond distance (Å)		Bond angle (°)	
Cu1 - Cu2	3.0278(7)	Cu1 - S1 - Cu2	82.24(3)
S1 - S2	3.1877(13)	Cu1 - S2 - Cu2	82.05(3)
Cu1 - S1	2.3022(10)	S1 - Cu1 - S2	87.48(4)
Cu1 - S2	2.3087(10)	S1 - Cu1 - N1	88.23(9)
Cu1 - N1	2.081(3)	S1 - Cu1 - N11	98.93(9)
Cu1 - N11	2.278(3)	S1 - Cu1 - N21	153.93(12)
Cu1 - N21	2.026(4)	S2 - Cu1 - N1	168.74(9)
		S2 - Cu1 - N11	111.43(9)
		S2 - Cu1 - N21	100.48(9)
Dihedral angle (°)		N1 - Cu1 - N11	79.53(12)
Cu1 - S1 - S2 - Cu2	–130.95(6)	N1 - Cu1 - N21	79.19(13)
Cu1 - S1 - Cu2 - S2	33.47(4)	N11 - Cu1 - N21	101.08(13)

symmetry operation * = 1–x, 1–y, 2–z

The other BF_4^- counterion is significantly disordered over at least three orientations.[6] The structure is highly similar to those of two reported μ-thiolate complexes $[Cu^{II}_2(\mathbf{L^{1*}S})_2](SbF_6)$ and $[Cu^{II}_2(\mathbf{L^2S})_2](BF_4)$ (Chapter 2).[1, 2] The Cu-Cu distances in $[Cu^{II}_2(\mathbf{L^{2*}S})_2]^{2+}$, $[Cu^{II}_2(\mathbf{L^{1*}S})_2]^{2+}$ and $[Cu^{II}_2(\mathbf{L^2S})_2]^{2+}$ are 3.03 Å, 2.94 Å and 3.04 Å respectively; the S-S distances are 3.19 Å, 3.13 Å and 3.16 Å. The folding angles of the Cu-S butterfly core over the S-S axis are 49°, 59° and 47°. In the structure of $[Cu^{II}_2(\mathbf{L^{2*}S})_2](BF_4)_2$ both methyl-substituted pyridyl rings are located at the same side of the Cu-S plane, as was found in the structure of $[Cu^{II}_2(\mathbf{L^2S})_2](BF_4)$.[1]

3.2.2 $[Cu^{I}_2Cu^{II}_2(\mathbf{L^{1*}S})_2(CH_3CN)_6]^{4+}$ and $[Cu^{II}_2(\mathbf{L^{2*}S})_2]^{2+}$ in Solution

Upon addition of two equivalents of $[Cu^{I}(CH_3CN)_4]^+$ to $\mathbf{L^{1*}SSL^{1*}}$ dissolved in CH_3CN, a solution containing $[Cu^{II}_2(\mathbf{L^{2*}S})_2]^{2+}$ is obtained, showing absorption bands at 248 nm ($\pi^* \leftarrow \pi$ pyridyl groups), 310 nm ($Cu^{II} \leftarrow$ S LMCT), 370 nm ($Cu^{II} \leftarrow$ S LMCT), as well as at 580, 785 and 910 nm (d-d transitions) as depicted in Figure 3.4a. Addition of two additional equivalents of $[Cu^{I}(CH_3CN)_4]^+$ leads to the formation of a brown solution from which $[Cu^{I}_2Cu^{II}_2(\mathbf{L^{1*}S})_2(CH_3CN)_6](BF_4)_4$ can be obtained. The UV-vis spectrum of $[Cu^{I}_2Cu^{II}_2(\mathbf{L^{1*}S})_2(CH_3CN)_6]^{4+}$ is almost identical to that of $[Cu^{II}_2(\mathbf{L^{1*}S})_2]^{2+}$ indicating that the Cu^{II} thiolate moiety is still present. This is confirmed by ^{1}H NMR spectroscopy (Figure 3.5); the resonances observed for $[Cu^{I}_2Cu^{II}_2(\mathbf{L^{1*}S})_2(CH_3CN)_6]^{4+}$ are similar to those for $[Cu^{II}_2(\mathbf{L^{1*}S})_2]^{2+}$, but are broadened indicating loss of the anti-ferromagnetic coupling between the two copper ions that occurs in $[Cu^{II}_2(\mathbf{L^{1*}S})_2]^{2+}$.

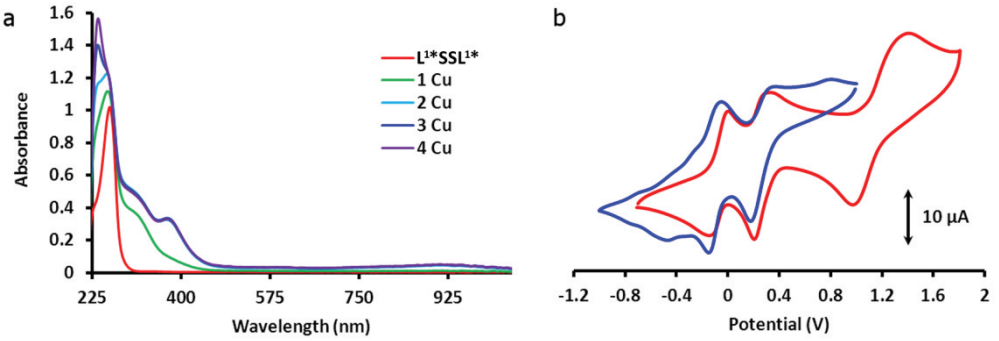

Figure 3.4: UV-vis spectra of $\mathbf{L^{1*}SSL^{1*}}$ (0.5 mM in CH_3CN) with 1, 2, 3 and 4 equivalents of $[Cu^{I}(CH_3CN)_4](BF_4)$ recorded with a transmission dipprobe set at a path length of 1.2 mm (a) and cyclic voltammograms of $\mathbf{L^{1*}SSL^{1*}}$ (0.5 mM) in CH_3CN with 2 equivalents (blue) and 4 equivalents (red) of $[Cu^{I}(CH_3CN)_4](BF_4)$ (b). Potentials are vs Ag/AgCl.

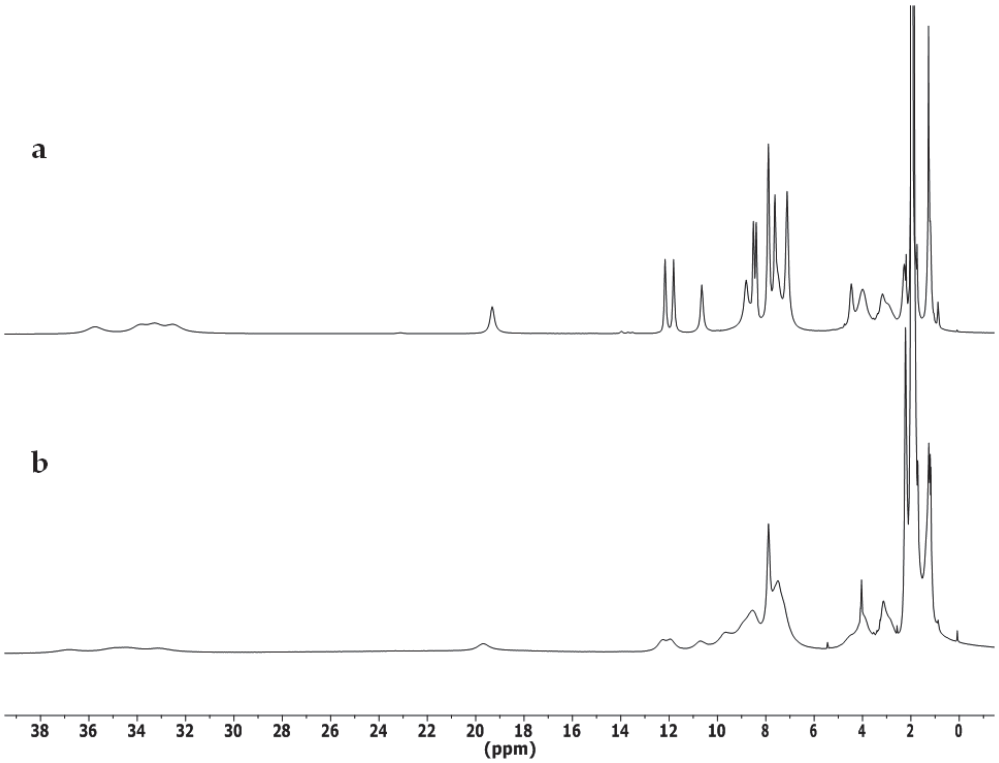

Figure 3.5: ^{1}H NMR spectra of $[Cu^{II}_2(\mathbf{L^{1*}S})_2]^{2+}$ (a) and $[Cu^{I}_2Cu^{II}_2(\mathbf{L^{1*}S})_2(CH_3CN)_6]^{4+}$ (b) in CD_3CN at RT.

Cyclic voltammetry has been carried out with both $[Cu^{II}_2(\mathbf{L^{1*}S})_2]^{2+}$ and $[Cu^{I}_2Cu^{II}_2(\mathbf{L^{1*}S})_2(CH_3CN)_6]^{4+}$; the voltammograms again show similarities (Figure 3.4b). The voltammogram of $[Cu^{II}_2(\mathbf{L^{1*}S})_2]^{2+}$ shows two quasi-reversible waves with $E_{1/2}$ of –0.10 V and 0.25 V and a number of less intense irreversible events. These waves are also present in the voltammogram of $[Cu^{I}_2Cu^{II}_2(\mathbf{L^{1*}S})_2(CH_3CN)_6]^{4+}$, although this species has an additional quasi-reversible wave (at $E_{1/2} \approx 1.20$ V) that can possibly be ascribed to the bridging $[Cu^{I}(CH_3CN)_2]^{+}$ moieties, as the oxidation of $[Cu^{I}(CH_3CN)_4]^{+}$ occurs at a comparable potential ($E_{1/2} = 1.10$ V; Figure AII.1, Appendix II). The ligand $\mathbf{L^{2*}SSL^{2*}}$ upon reaction with Cu^{I} forms a Cu^{II} μ-thiolate compound in both dichloromethane and acetone solutions, which is confirmed by the X-ray structure determination of $[Cu^{II}_2(\mathbf{L^{2*}S})_2](BF_4)_2$ (Section 3.2.1) and the UV-vis spectrum of the dark-green species in dichloromethane (Figure AII.2a, Appendix II). In acetonitrile, however, a light greenish-yellow solution arises after addition of Cu^{I},

which can be attributed to the formation of the disulfide compound $[Cu^{I}_2(\mathbf{L^{2*}SSL^{2*}})]^{2+}$, based on the UV-vis spectra (Figure AII.2b, Appendix II).
Similar behavior has been reported for $\mathbf{L^2SSL^2}$ (Chapter 2).[1] ^{1}H NMR spectra of both the Cu^{I} disulfide and the anti-ferromagnetically coupled Cu^{II} thiolate complex of $\mathbf{L^{2*}SSL^{2*}}$ are shown in Figure 3.6.

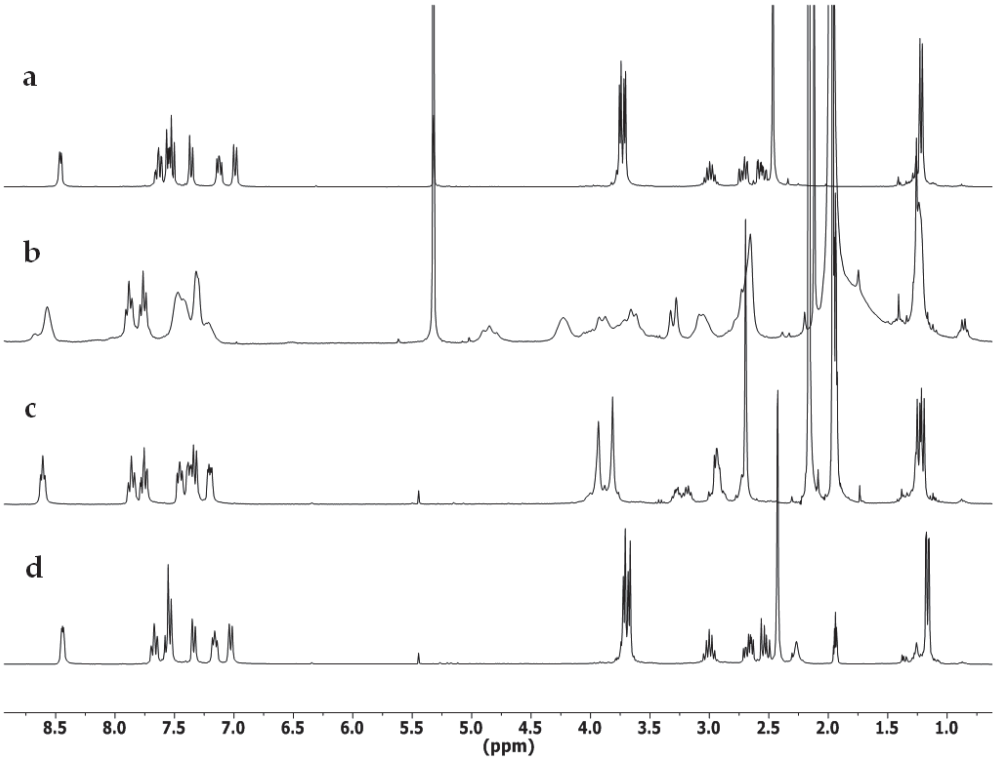

Figure 3.6: ^{1}H NMR spectra of $\mathbf{L^{2*}SSL^{2*}}$ (a) and $[Cu^{II}_2(\mathbf{L^{2*}S})_2]^{2+}$ (b) in CD_2Cl_2 and $\mathbf{L^{2*}SSL^{2*}}$ (d) and $[Cu^{I}_2(\mathbf{L^{2*}SSL^{2*}})]^{2+}$ (c) in CD_3CN at RT.

3.2.3 Spectroscopic Analysis of the Proton-Induced Conversion

Upon addition of protons to an acetonitrile solution of $[Cu^{II}_2(\mathbf{L^{1*}S})_2]^{2+}$ a color change occurs, as has been reported by Stack and coworkers.[2] The addition of 1 – 4 equivalents of HBF_4 (in ratio to the ligand) to the Cu^{II} μ-thiolate containing solution was monitored with ^{1}H NMR; the results are depicted in Figure 3.7. Addition of one equivalent of H^+ leads to broadening of the peaks and a shift of all resonances to the diamagnetic region. Addition of more protons leads to sharper peaks, resulting in a sharp diamagnetic spectrum after addition of four equivalents of protons. This

spectrum is identical with that of the protonated disulfide ligand (Figure 3.8), revealing that the ligand has dissociated giving $[H_4\mathbf{L^{1*}SSL^{1*}}]^{4+}$ and $[Cu^{I}(CH_3CN)_4]^{+}$. The effect of the addition of protons to $[Cu^{II}_2(\mathbf{L^{1*}S})_2]^{2+}$ was also monitored using UV-vis (Figure 3.9a). The addition of two equivalents of acid results not only in the disappearance of the d-d transitions, but also in the disappearance of the $Cu^{II} \leftarrow S$ LMCT band. We would expect to see an $S \leftarrow Cu^{I}$ MLCT band if redox isomerisation to the Cu^{I} disulfide would occur,[1, 7] and its absence indicates that the sulfur center is no longer bound to copper and might be protonated. Again, the UV-vis spectrum of the disulfide ligand in the presence of two equivalents of acid is identical (Figure AII.3, Appendix II). Addition of stoichiometric amounts of NEt_3 completely reverses the reaction, regenerating the Cu^{II} thiolate complex.

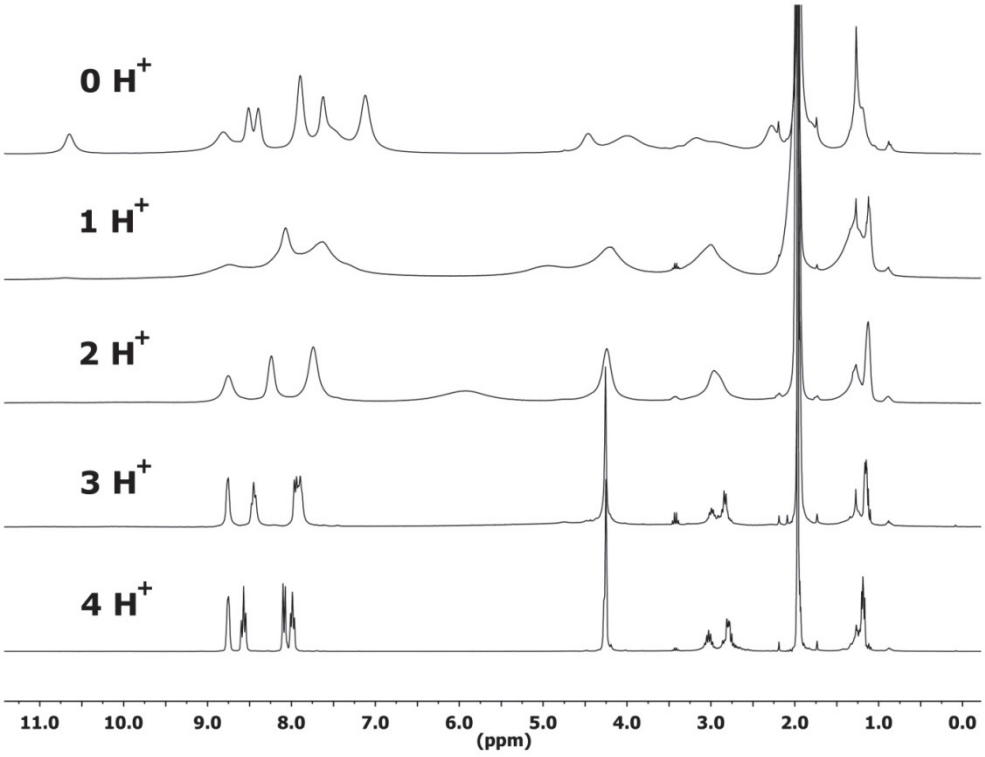

Figure 3.7: ^{1}H NMR spectra of $[Cu^{II}_2(\mathbf{L^{1*}S})_2]^{2+}$ with 0 - 4 equivalents of $HBF_4{\cdot}Et_2O$ in CD_3CN at RT.

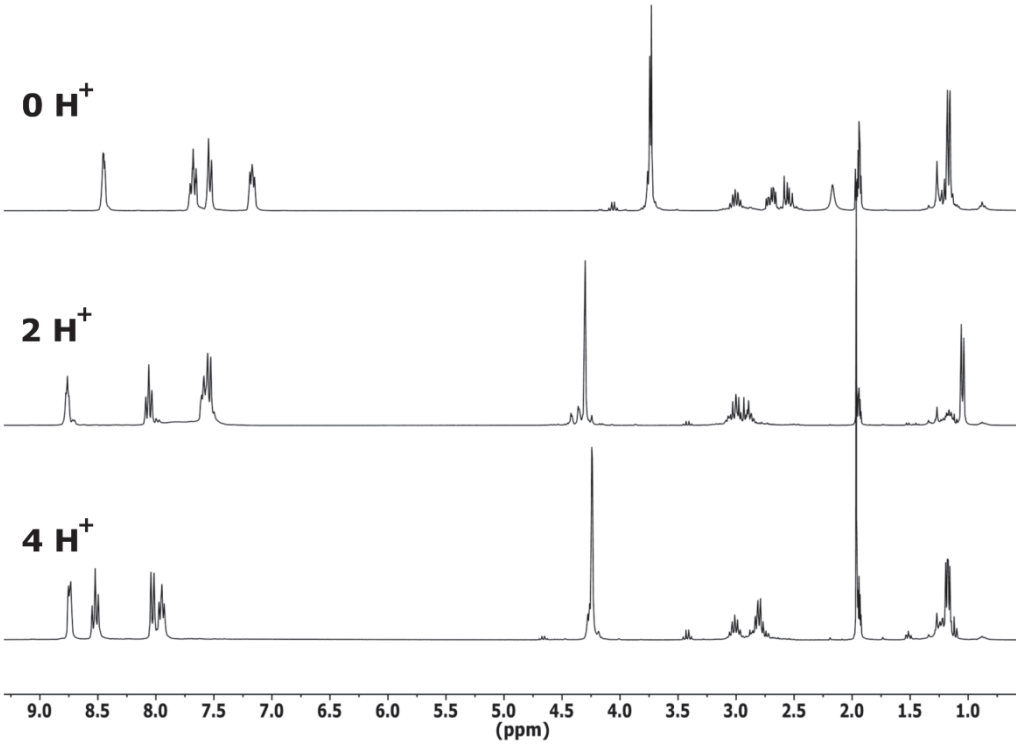

Figure 3.8: ^{1}H NMR spectra of **L^{1}*SSL^{1}*** with 0 - 4 equivalents of $HBF_4 \cdot Et_2O$ in CD_3CN at RT.

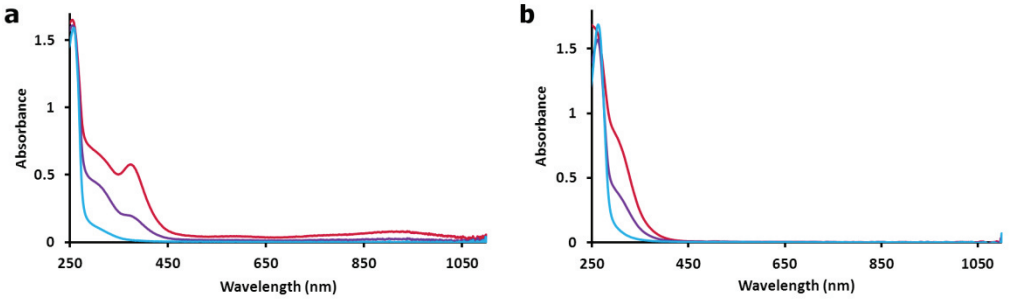

Figure 3.9: UV-vis spectra of $[Cu^{II}_2(\mathbf{L^{1*}S})_2]^{2+}$ (a) and $[Cu^{I}_2(\mathbf{L^{2*}SSL^{2*}})]^{2+}$ (b) with 0 equivalents (red line), 1 equivalent (purple line) and 2 equivalents (blue line) of $HBF_4 \cdot Et_2O$ in CH_3CN at 2 mM [Cu] recorded with a transmission dipprobe set at a path length of 1.2 mm.

Stack et.al.[2] used trifluoridomethanesulfonic acid (HOTf) as the proton source instead of HBF_4. We repeated our experiments with HOTf; the same spectra were obtained as reported by the group of Stack, however, we find that upon addition of HOTf the reaction does not occur stoichiometrically. More HOTf is needed to obtain the same

results as with 4 equiv. HBF_4, as was found with both UV-vis and NMR spectroscopy (Figure AII.5 and AII.7, Appendix II). The use of a solvent that is more easily protonated, such as methanol or acetone, also leads to more gradual protonation of the complex.

As the ligand **L²*SSL²*** can form either the Cu^{I} disulfide or the Cu^{II} thiolate complex depending on the solvent, it is ideally suited to study the effect of protonation of the Cu^{II} or Cu^{I} compounds separately. Addition of just one equivalent of HBF_4 to $[Cu^{II}_2(\mathbf{L^{2*}S})_2]^{+}$ in dichloromethane already leads to precipitation of protonated ligand (Figure AII.6, Appendix II). Upon addition of two equivalents of HBF_4 to $[Cu^{I}_2(\mathbf{L^{2*}SSL^{2*}})]^{2+}$ in acetonitrile again the S ← Cu^{I} MLCT band disappears indicating ligand dissociation (Figure 3.9b).

3.2.4 DFT Analysis of the Proton-Induced Conversion

The experimental and spectroscopic results indicate that addition of two equivalents of protons to $[Cu^{II}_2(\mathbf{L^{1*}S})_2]^{2+}$ leads to ligand dissociation and formation of a mixed-valent tetranuclear cluster, instead of conversion to a protonated Cu^{I} disulfide complex as suggested by Stack et al.[2] However, as the experimental data are not conclusive, we decided to study these complexes computationally with DFT. The calculations were carried out as reported by us recently,[1] taking into account the anti-ferromagnetic coupling between the two Cu^{II} ions in the μ-thiolate complex (Section 3.5.3). Due to the presence of the methyl groups next to the sulfur atom, the ligand **L¹*SSL¹*** has four diastereoisomers (*RR*, *SS*, *RS*, *SR*), which leads to the potential formation of three chemically distinguishable complexes (**X**, **Y** and **Z**, see Figure 3.11). The calculated structures of the three different complexes of the Cu^{II} thiolate complexes (**A**, Figure 3.10) are shown in Figure 3.11 and the relative energies of formation for **A**, **B** and **C** in conformation **X**, **Y** and **Z** are given in Table 3.4. The most stable *RR*/*SS* and *RS*/*SR* thiolate and disulfide complexes were used for the calculations including added protons.

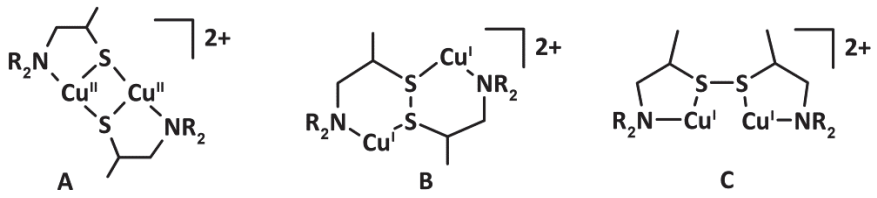

Figure 3.10: Schematic representation of the copper complexes in Cu^{II} μ-thiolate (**A**), Cu^{I} *transoid*-disulfide (**B**) or Cu^{I} *cisoid*-disulfide (**C**) conformation. R = 2-pyridylmethyl.

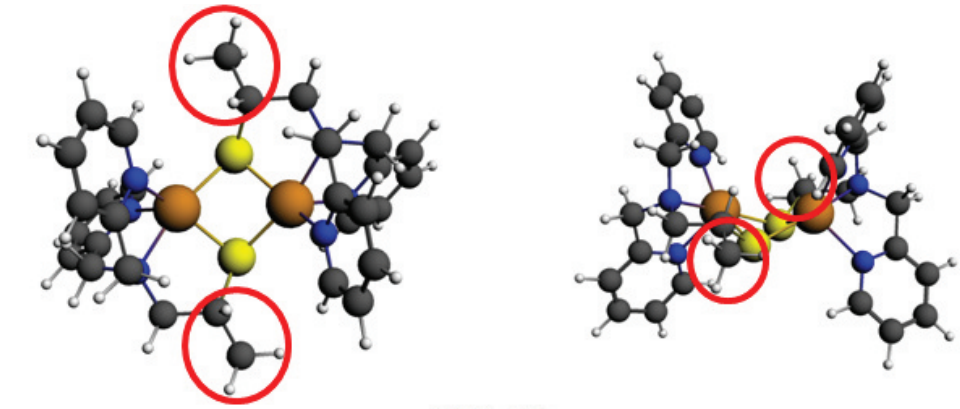

X: *RR* / *SS*
0 kJ mol^{-1}

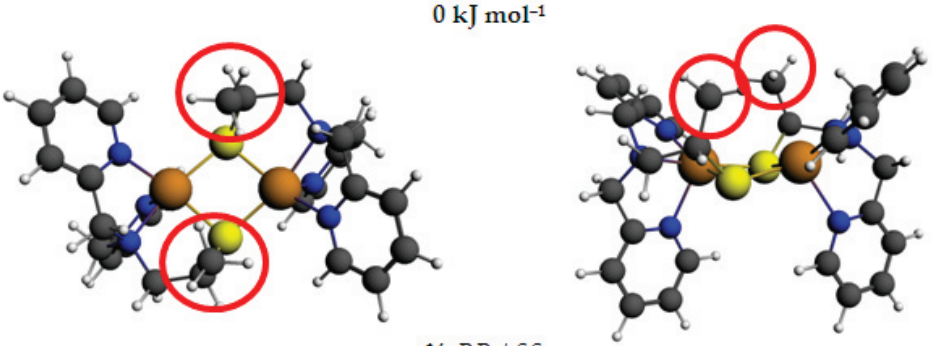

Y: *RR* / *SS*
+43 kJ mol^{-1}

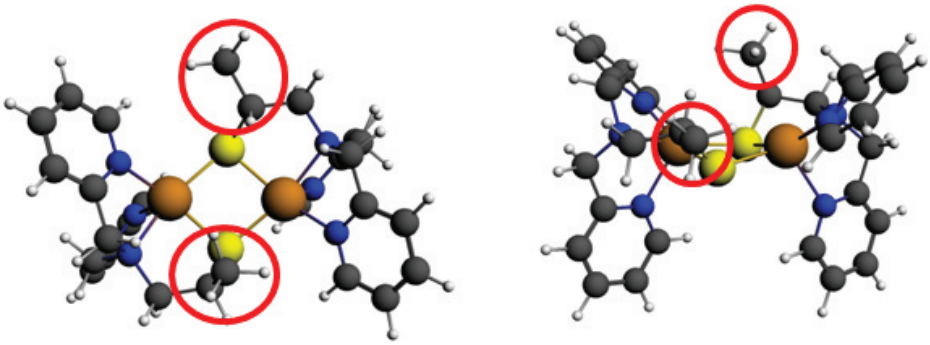

Z: *RS* / *SR*
+31 kJ mol^{-1}

Figure 3.11: Optimized geometries for three chemically distinguishable $[Cu^{II}_2(\mathbf{L^{1*}S})_2]^{2+}$ complexes (**X**; **Y** and **Z**) and their relative energies computed at ZORA-OPBE/TZ2P solvated in CH_3CN (COSMO).

Although it is likely that the pyridyl nitrogen atoms of the ligand are protonated,[2] protonation of the thiolate and tertiary amine atoms were considered as well. The energies of all optimized protonated complexes are given in Table AII.1, Appendix II. The calculations confirm that the pyridyl nitrogen atoms are the most likely site of protonation, as these structures result in the lowest energies. The calculated energies of the protonated μ-thiolate complexes (**A**) and the protonated disulfide complexes (*transoid* **B** and *cisoid* **C**, see Figure 3.10) with or without coordinated acetonitrile molecules are collected in Table 3.5.

A graphical representation of the calculated energies is depicted in Figure 3.12. The calculations show that the protonated disulfide complexes in both geometries (**B** and **C**) with and without coordinated acetonitrile are higher in energy than the protonated Cu^{II} μ-thiolate complex, indicating that formation of a protonated Cu^{I} disulfide species is thermodynamically unfavorable. Ligand dissociation is favored by more than 100 kJ mol^{-1}, supporting that this readily occurs upon protonation.

Table 3.4: Relative formation energies (kJ mol^{-1}) for Cu^{II} μ-thiolate (**A**) and Cu^{I} disulfide (**B** and **C**) complexes in three geometries (**X**, **Y** and **Z,** Figure 3.11) computed at ZORA-OPBE/TZ2P solvated in CH_3CN (COSMO).

	X: *RR* / *SS*	**Y: RR/*SS***	**Z: *RS* / *SR***
L¹*SSL¹* + 2 $[Cu(CH_3CN)_4]^+$	**0**	**0**	4
A + 8 CH_3CN	−94	−51	−64
B + 8 CH_3CN	−88	−54	−76
C + 8 CH_3CN	−70	−77	−77

Table 3.5: Geometry optimization energies (kJ mol^{-1}) for protonated Cu^{II} μ-thiolate (**A**) and Cu^{I} disulfide (**B** and **C**) complexes and protonated ligand **L¹*SSL¹*** computed at ZORA-OPBE/TZ2P in acetonitrile (COSMO).

	Conformation *RR* / *SS*	**Conformation *RS* / *SR***
[**A** + 2 H^+]$^{4+}$ + 8 CH_3CN	**0**	18
[**B** + 2 H^+]$^{4+}$ + 8 CH_3CN	27	30
[**B** + 2 H^+ + 2 CH_3CN]$^{4+}$ + 6 CH_3CN	20	38
[**C** + 2 H^+]$^{4+}$ + 8 CH_3CN	57	51
[**C** + 2 H^+ + 2 CH_3CN]$^{4+}$ + 6 CH_3CN	23	6
[**L¹*SSL¹*** + 2 H^+]$^{2+}$ + 2 $[Cu^I(CH_3CN)_4]^+$	−109	−114

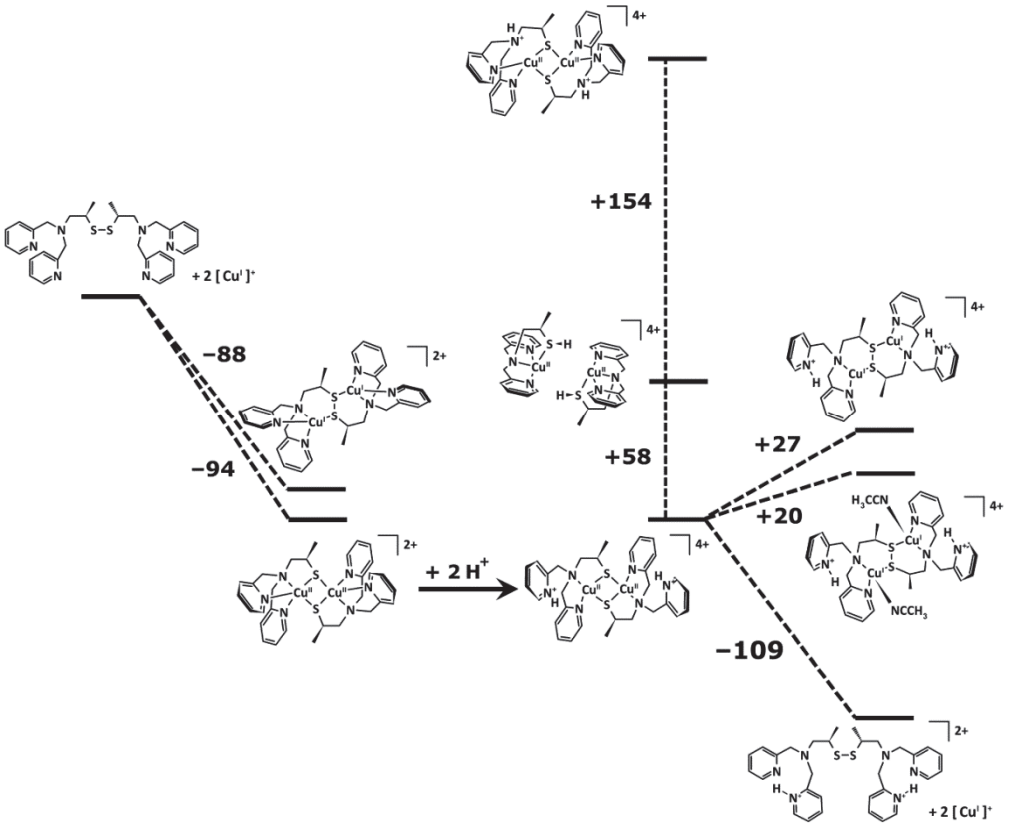

Figure 3.12: Schematic representation of the energies calculated for copper complexes with **L¹*SSL¹*** in the *RR/SS* conformation. For clarity only the *transoid* structures **B** are shown and non-coordinated CH_3CN molecules are omitted.

3.3 Discussion

UV-vis spectra of the titration of $[Cu^{II}_2(\mathbf{L^{1*}S})_2]^{2+}$ with HBF_4 revealed the disappearance of the Cu^{II} d-d transitions and the absence of an S ← Cu^{I} MLCT band after addition of only two equivalents of acid, indicating that the sulfur center no longer binds to copper. Addition of two equivalents of acid to the related compound $[Cu^{II}_2(\mathbf{L^{2*}S})_2]^{2+}$ in dichloromethane resulted in precipitation of $[H_4\mathbf{L^{2*}SSL^{2*}}]^{4+}$, whereas addition to the redox-isomeric compound $[Cu^{I}_2(\mathbf{L^{2*}SSL^{2*}})]^{2+}$ in acetonitrile resulted in disappearance of the S ← Cu^{I} MLCT band similar as observed for $[Cu^{II}_2(\mathbf{L^{1*}S})_2]^{2+}$. The spectroscopic results thus suggest that upon protonation of $[Cu^{II}_2(\mathbf{L^{1*}S})_2]^{2+}$, ligand dissociation takes place via conversion to a Cu^{I} disulfide complex. Crystallization of the complex $[Cu^{I}_2Cu^{II}_2(\mathbf{L^{1*}S})_2(CH_3CN)_6](BF_4)_4$ upon the addition of two equivalents of protons to a solution of $[Cu^{II}_2(\mathbf{L^{1*}S})_2]^{2+}$ suggests that the liberated Cu^{I} acetonitrile

complex, formed after dissociation of the protonated ligand, is accommodated by the remaining Cu^{II} thiolate compound.

Monitoring the titration of H^+ to $[Cu^{II}_2(\mathbf{L^{1*}S})_2]^{2+}$ with ^1H NMR spectroscopy showed the formation of fully protonated ligand after addition of four equivalents of HBF_4. After addition of two equivalents of HBF_4 the ^1H NMR spectrum shows rather broad signals in the diamagnetic region, indicating the presence of a number of different species, which may include an equilibrium between the doubly protonated complex, $[H_4\mathbf{L^{1*}SSL^{1*}}]^{4+}$ and $[Cu^{I}_2Cu^{II}_2(\mathbf{L^{1*}S})_2(CH_3CN)_6]^{4+}$ species. Despite the use of different acids our ^1H NMR spectra are highly similar to those reported by Stack and coworkers. It must be noted that Stack and coworkers have not added more than three equivalents of HOTf in any of their experiments. Even though HOTf is a stronger acid than HBF_4 in water, the acidity could be reversed in acetonitrile as indicated by our experiments. In our experience, OTf^- coordinates more strongly to copper than BF_4^- which suggests weaker acidity of the OTf^- ion in acetonitrile.[3]

The optimized energies calculated using DFT (Table 3.5) show that protonation of the pyridyl nitrogen is most favorable, which was also concluded by Stack and coworkers based on the results of ^1H NMR NOE enhancements.[2] However, the observation of a proton at a pyridine nitrogen with NMR techniques does not tell whether a protonated complex or just a protonated ligand is formed. More importantly, our calculations show that the protonated Cu^{II} thiolate complex is lower in energy than the protonated Cu^{I} disulfide complex, with or without coordination of acetonitrile. Ligand dissociation, on the other hand, is favored by more than 100 kJ mol^{-1}, thus clarifying the experimental results that suggest loss of the copper-sulfur interaction. This means that addition of just two protons per dinuclear copper compound already leads to ligand dissociation for both the Cu^{II} thiolate and the Cu^{I} disulfide complexes.

These proton-coupled reactions form a model for the biological systems, since these Cu^{II} μ-thiolate complexes show resemblance to the Cu_A site. Studies on the Cu_A site in cytochrome *c* oxidase and the artificially engineered Cu_A site in azurin have shown that these active sites are very sensitive to pH changes.[8-12] It is hypothesized that protonation of the Cu_A site induces ligand dissociation of one of the equatorial histidine ligands, which possibly leads to a change in valence state of the copper ions. Furthermore, understanding of this pH dependent behavior can be of importance for other pyridyl-containing metal complexes, which are used as catalysts for reactions such as water oxidation,[13] proton reduction[14] and CO_2 reduction.[15-17] This study shows that the pH can have a large effect on the coordination environment of the metal and might affect the reactivity of the metal center or the mechanism of catalysis.

3.4 Conclusion

We have found that after addition of only two equivalents of protons, a potentially octadentate ligand dissociates from two copper ions, after an intramolecular redox reaction of a dinuclear Cu^{II} dithiolate species to form $[Cu^{I}(CH_3CN)_4]^+$ and the protonated disulfide ligand. Ligand dissociation was found to take place when adding protons to either the Cu^{II} μ-thiolate compound $[Cu^{II}_2(\mathbf{L^{2*}S})_2]^{2+}$ or the Cu^{I} disulfide compound $[Cu^{I}_2(\mathbf{L^{2*}SSL^{2*}})]^{2+}$, showing that this dissociation also readily occurs for Cu^{I} disulfide complexes. Our findings are in contrast to an earlier report describing redox isomerization to a Cu^{I} disulfide species that is protonated at the pyridyl moieties. In the earlier report HOTf was used instead of HBF_4 and although we obtained similar ^{1}H NMR and UV-vis spectra, we found that HOTf is a weaker acid in acetonitrile and does not react stoichiometrically with $[Cu^{II}_2(\mathbf{L^{1*}S})_2]^{2+}$. Our results show that the addition of protons can have an immense effect on the coordination environment of copper ions. The presence of small amounts of acid can already lead to ligand dissociation and possible electron-transfer. The relevance of our findings stretches from biological systems to the field of inorganic chemistry and catalysis. It is of the utmost importance to point out that already small changes in pH may have a significant impact on the coordination environment of the actual catalyst or complex structure in solution.

3.5 Experimental Section

3.5.1 General Methods

Reagents and solvents were purchased from commercial sources. The syntheses of all copper complexes were carried out using standard Schlenk-line techniques under an argon atmosphere. Solvents were distilled and deoxygenated by bubbling a stream of argon through the solution and were stored on activated molecular sieves under argon prior to use. $[Cu^{I}(CH_3CN)_4](BF_4)$ and 1-(6-methyl-2-pyridinyl)-*N*-(2-pyridinylmethyl)methanamine and $[Cu^{II}_2(\mathbf{L^{1*}S})_2]^{2+}$ were synthesized according to literature procedures.[2, 18, 19] NMR spectra were recorded on a Bruker 300 DPX spectrometer. NMR experiments under argon were carried out using a J. Young NMR tube. IR spectra were obtained on a Perkin Elmer UATR (Single Reflection Diamond) Spectrum Two device (4000-700 cm^{-1}; resolution 4 cm^{-1}). Mass spectrometry was measured using a Finnigan Aqua Mass Spectrometer (MS) with electro spray ionization (ESI). Sample introduction was achieved through a Dionex ASI-100 automated sample injector with an eluent flow rate of 0.2 mL/min. Elemental analyses were performed using a Perkin Elmer 2400 Series II CHNS/O analyzer. UV-vis spectra were collected using a transmission dipprobe with variable path length on an Avantes Avaspec-2048 spectrometer with Avalight-DH-S-BAL light source. Cyclic voltammetry was performed with an Autolab PGstat10 potentiostat controlled by GPES4 software. A three electrode arrangement with a

glassy carbon working electrode (3 mm diameter), an Ag/AgCl double junction reference electrode and a Pt wire counter electrode were used in different solvents with 0.1 M NBu_4PF_6 as the electrolyte. In these conditions the Fc/Fc^+ couple was found to be located at +442 mV with a peak-to-peak separation of 60 mV in CH_3CN, and at + 461 mV with a peak-to-peak separation of 92 mV in dichloromethane. Potentials are given relative to the Ag/AgCl electrode.

3.5.2 Single Crystal X-ray Crystallography

All reflection intensities at 100(2) K for $[Cu^{I}_2Cu^{II}_2(\mathbf{L^{1}*S})_2(CH_3CN)_6](BF_4)_4$ were measured and at 110(2) K for $[Cu^{II}_2(\mathbf{L^{2}*S})_2](BF_4)_2$ using a SuperNova diffractometer (equipped with Atlas detector) with Cu $K\alpha$ radiation (mirror optics, λ = 1.54178 Å) under the program CrysAlisPro (Versions 1.171.36.2424 or 1.171.36.32 Agilent Technologies, 2012-2013). The same program was also used to refine the cell dimensions and for data reduction. The structure was solved with the program SHELXS-2013 (Sheldrick, 2013)[20] and was refined on F^2 with SHELXL-2013 (Sheldrick, 2013).[20] Analytical numeric absorption corrections based on a multifaceted crystal model were applied using CrysAlisPro. The temperature of the data collection was controlled using the system Cryojet (manufactured by Oxford Instruments). The H atoms were placed at calculated positions using the instructions AFIX 13, AFIX 23, AFIX 43 or AFIX 137 with isotropic displacement parameters having values 1.2 or 1.5 times *U*eq of the attached C atoms. For the refinement of $[Cu^{II}_2(\mathbf{L^{2}*S})_2](BF_4)_2$, some unresolved electron density – *i.e.*, possibly some amount of disordered solvent molecule (the unresolved electron density did not indicate any additional component of disorder BF_4^-) – has been taken out in the final refinement (SQUEEZE details are provided in the CIF file).

3.5.3 DFT Calculations

All calculations were performed with the Amsterdam Density Functional (ADF) program,[21, 22] using relativistic DFT at ZORA OPBE/TZ2P for geometry optimization and energies.[23] Solvation in acetonitrile was simulated using the conductor-like screening model (COSMO).[24-27] All stationary points in the condensed phase were verified to be minima on the potential energy surface (PES) through vibrational analysis. The energies of the singlet state of the Cu^{II} μ-thiolate complexes (E^S) have been obtained from the unrestricted broken-symmetry singlet energies (E^{BS}) and the energy of the triplet (E^T) with the approximate projection method of Noodleman: $E^S = 2E^{BS} - E^T$.[28, 29]

Some systems were optimized in C_2 symmetry (see Supporting Information). CH_3CN was optimized with C_{3v} symmetry.

3.5.4 Ligand and complex synthesis

L¹*SSL¹*

This ligand was synthesized using a combination of reported syntheses.[2-4] Di-(2-pyridylmethyl)amine (2.0 mL, 11.0 mmol) was dissolved in 10 ml CH_3CN under argon.

Propylene sulfide (1.3 mL, 16.5 mmol) was added, after which the reaction mixture was stirred for 15 hours at 70 °C under argon. After the mixture had cooled down, the solvent and excess propylene sulfide were evaporated. The resulting orange oil was dissolved in 20 mL methanol and titrated with 0.5 M iodine in methanol until a brown color persisted. The reaction was quenched with $NaHSO_3$ (10% in H_2O) regaining the yellow color. The solvent was evaporated and 50 mL H_2O was added. 2 M NaOH was added until pH > 10. The water layer was extracted with 3 x 50 mL $CHCl_3$, the organic layer was dried over Na_2SO_4 and evaporated to yield a brown/yellow oil. The resulting oil was purified by column chromatography (basic alumina, eluent 60% EtOAc in petroleum ether) which yielded a light yellow oil as a mixture of of (*R*,*R*), (*S*,*S*), and (*R*,*S*) stereoisomers (2.69 g, 4.9 mmol, 90%). ^{1}H-NMR (300 MHz, CD_3CN, RT): δ 1.15 (s, 3H, C*-CH_3), 1.17 (s, 3H, C*-CH_3), 2.55 (dd, *J* = 13 Hz, 7.8 Hz, 2H, N-CH_2-C*), 2.70 (m, 2H, N-CH_2-C*), 3.01 (quin, *J* = 6.6 Hz, 2H, C*-*H*), 3.73 (s, 4H, Py-CH_2-N), 3.74 (s, 4H, Py-CH_2-N), 7.14 (m, 4H, Py-H_5), 7.53 (m, 4H, Py-H_3), 7.65 (tt, *J* = 7.5 Hz, 1.8 Hz, 1.5 Hz, 4H, Py-H_4), 8.44 (m, 4H, Py-H_6). ^{13}C-NMR (75 MHz, CD_3CN, RT): δ 19.2 (C*-*C*H$_3$), 19.3 (C*-*C*H$_3$), 45.3 (*C**), 45.4 (*C**), 60.8 (N-*C*H$_2$-C*), 61.0 (N-*C*H$_2$-C*), 61.3 (Py-*C*H$_2$-N), 61.4 (Py-*C*H$_2$-N), 123.0 (Py-*C*$_5$), 124.1 (Py-*C*$_3$), 124.1 (Py-*C*$_3$), 137.2 (Py-*C*$_4$), 149.8 (Py-*C*$_6$), 160.4 (Py-*C*$_2$), 160.5 (Py-*C*$_2$). ESI-MS found (calcd) for $[M + H]^+$: *m*/*z* 545.2 (545.3).

*L²*SSL²**

This ligand was synthesized in a similar way as ligand **L¹*SSL¹*** starting from 1-(6-methyl-2-pyridyl)-*N*-(2-pyridylmethyl)methanamine (3.56 g, 16.7 mmol) dissolved in 25 mL CH_3CN under argon. Propylene sulfide (2.0 mL, 25.0 mmol) was added, after which the reaction mixture was stirred for 3 days at 70 °C under argon. Further workup and reaction with I_2 was done in the same way as for **L¹*SSL¹***. The product was obtained after column chromatography (basic alumina, eluent 20% → 100% EtOAc in petroleum ether) as a yellow oil (1.12 g, 2.0 mmol, 23%). ^{1}H-NMR (300 MHz, CD_3CN, RT): δ 1.15 (d, *J* = 2.1 Hz, 3H, C*-CH_3), 1.18 (d, *J* = 2.4 Hz, 3H, C*-CH_3), 2.42 (s, 3H, Py-CH_3), 2.43 (s, 3H, Py-CH_3), 2.53 (dd, *J* = 13 Hz, 7.8 Hz, 2H, N-CH_2-C*), 2.67 (m, 2H, N-CH_2-C*), 3.00 (quin, *J* = 6.9 Hz, 2H, C*-*H*), 3.67 (s, 2H, Py$_{Me}$-CH_2-N), 3.68 (s, 2H, Py-CH_2-N), 3.71 (s, 2H, Py$_{Me}$-CH_2-N), 3.72 (s, 2H, Py-CH_2-N), 7.03 (d, *J* = 7.5 Hz, 2H, Py$_{Me}$-H_3), 7.16 (tt, *J* = 6.0 Hz, 1.5 Hz, 1.2 Hz, 2H, Py$_{Me}$-H_4), 7.34 (d, *J* = 7.5 Hz, 2H, Py-H_3), 7.55 (t, *J* = 7.8 Hz, 4H, Py$_{Me}$-H_5; Py-H_4), 7.67 (t, *J* = 7.8 Hz, 2H, Py-H_5), 8.44 (m, 2H, Py-H_6). ^{13}C-NMR (75 MHz, CD_3CN, RT): δ 19.1 (C*-*C*H$_3$), 19.2 (C*-*C*H$_3$), 24.5 (Py-*C*H$_3$) 45.2 (*C**), 45.4 (*C**), 60.7 (Py$_{Me}$-*C*H$_2$-N), 60.9 (Py-*C*H$_2$-N), 61.3 (N-*C*H$_2$-C*), 61.3 (N-*C*H$_2$-C*), 61.4 (N-*C*H$_2$-C*), 61.4 (N-*C*H$_2$-C*), 120.8 (Py-*C*$_5$), 120.9 (Py-*C*$_5$), 122.2 (Py$_{Me}$-*C*$_5$), 123.0 (Py$_{Me}$-*C*$_3$), 124.0 (Py-*C*$_3$), 124.1 (Py-*C*$_3$), 137.2 (Py$_{Me}$-*C*$_4$), 137.5 (Py-*C*$_4$), 149.7 (Py-*C*$_6$), 158.3 (Py$_{Me}$-*C*$_2$), 159.7 (Py$_{Me}$-*C*$_6$), 159.7 (Py$_{Me}$-*C*$_6$), 160.4 (Py-*C*$_2$), 160.5 (Py-*C*$_2$). ESI-MS found (calcd) for $[M + H]^+$: *m*/*z* 573.1 (573.3); $[M + Na]^+$: *m*/*z* 595.1 (595.3). IR (neat, cm^{-1}): 1590s, 1577s, 1456m, 1433s, 1365m, 1152m, 1084m, 994s, 976m, 785s, 756m, 614s.

$[Cu^{I}_2Cu^{II}_2(\mathbf{L^{1}*S})_2(CH_3CN)_6](BF_4)_4$

L^{1}*SSL^{1}* (19.8 mg, 0.04 mmol) was dissolved in CH_3CN (4.0 ml). To this solution $[Cu^{I}(CH_3CN)_4](BF_4)$ (46.1 mg, 0.15 mmol) was added, which resulted in a dark brown solution. The solution was stirred for 1 hour after which the solution was added slowly to 100 mL diethyl ether while stirring vigorously. A very oxygen-sensitive greyish purple solid was collected by filtration (41.0 mg, 0.03 mmol, 81%). This compound turned light green when put under vacuum. Crystals suitable for X-ray structure determination were obtained by vapor diffusion of diethyl ether into an CH_3CN solution containing 1 equivalent of **L^{1}*SSL^{1}***, 2 equivalents of $[Cu(CH_3CN)_4](BF_4)$ and 2 equivalents of $HBF_4{\cdot}Et_2O$. Elemental analysis calcd for $C_{30}H_{36}B_4Cu_4F_{16}N_6S_2$ + 2 H_2O: C 30.48, H 3.41, N 7.11, S 5.42. Found: C 29.29, H 3.45, N 6.99, S 5.42. ESI-MS found (calcd) for $[Cu(CH_3CN)_2]^+$: *m/z* 145.1 (145.0); $[Cu(CH_3CN)_3]^+$: *m/z* 186.0 (186.0); [Cu(**L^{1}*S**) – S]$^+$: *m/z* 303.0 (303.1); [Cu(**L^{1}*S**)]$^+$: *m/z* 335.0 (335.1). UV-vis in CH_3CN at 0.5 mM complex concentration: 235 nm (ε = 7000 M^{-1} cm^{-1}), 255 nm (ε = 6150 M^{-1} cm^{-1}), 308 nm (ε = 2500 M^{-1} cm^{-1}), 372 nm (ε = 1700 M^{-1} cm^{-1}), 580 nm (ε = 170 M^{-1} cm^{-1}), 910 nm (ε = 250 M^{-1} cm^{-1}).

$[Cu^{II}_2(\mathbf{L^{2}*S})_2](BF_4)_2$

L^{2}*SSL^{2}* (92.5 mg, 0.16 mmol) was dissolved in acetone (10 ml). To this solution $[Cu^{I}(CH_3CN)_4](BF_4)$ (101 mg, 0.32 mmol) was added, which resulted in a very dark green solution. This solution was stirred for 1 hour after which it was added to 20 mL pentane resulting in a grey powder (88.3 mg, 0.10 mmol, 63%) after filtration. Crystals suitable for X-ray structure determination were obtained by slow vapor diffusion of pentane in an acetone solution containing the complex. ^{1}H NMR (300 MHz, CD_2Cl_2, RT): δ 1.24 (br, 3H, C*-CH_3), 1.26 (s, 3H, C*-CH_3), 2.66 (br, 6H, Py-CH_3), 3.07 (d, *J* = 9.9 Hz, 2H, N-CH_2-C*), 3.30 (d, *J* = 14 Hz, 2H, N-CH_2-C*), 3.76 (m, 6H), 4.23 (br, 2H), 4.86 (t, *J* = 18 Hz, 2H), 7.21 (br, 2H), 7.32 (br, 2H), 7.45 (br, 4H), 7.77 (t, *J* = 7.5 Hz, 2H), 7.88 (t, *J* = 7.5 Hz, 2H), 8.57 (br, 2H, Py-H_6). ESI-MS found (calculated) for [**L^{2}*SSL^{2}*** + Cu]$^{2+}$: *m/z* 317.1 (317.6); $[Cu_2(\mathbf{L^{2}*S})_2]^{2+}$: *m/z* 349.1 (349.1); [**L^{2}*SSL^{2}*** + 3 Cu]$^{2+}$: *m/z* 381.0 (381.5); [**L^{2}*SSL^{2}*** + Cu]$^+$: *m/z* 635.1 (635.2); $[M - BF_4]^+$: *m/z* 785.1 (785.1). UV-vis in dichloromethane at 2 mM [Cu]: 263 nm (ε = 6800 M^{-1} cm^{-1}), 296 nm (ε = 4500 M^{-1} cm^{-1}), 600 nm (ε = 125 M^{-1} cm^{-1}). IR (neat, cm^{-1}): 1607s, 1577s, 1466m, 1445m, 1050w, 868s, 766m, 620s.

$[Cu^{I}_2(\mathbf{L^{2}*SSL^{2}*})](BF_4)_2$

L^{2}*SSL^{2}* (5.73 mg, 0.01 mmol) was dissolved in CH_3CN (2 ml). To this solution was added $[Cu(CH_3CN)_4](BF_4)$ (6.29 mg 0.02 mmol), resulting in a light greenish yellow solution. Attempts to isolate the complex resulted in the formation of oil. ^{1}H NMR (300 MHz, CD_3CN, RT): δ 1.20 (d, *J* = 6.9 Hz, 3H, C*-CH_3), 1.24 (d, *J* = 6.9 Hz, 3H, C*-CH_3), 2.70 (s, 6H, Py-CH_3), 2.94 (m, 4H, N-CH_2-C*), 3.18 (m, 1H, C*-*H*), 3.27 (m, 1H, C*-*H*), 3.82 (s, 4H, Py_{Me}-CH_2-N), 3.93 (s, 4H, Py-CH_2-N), 7.20 (dd, *J* = 7.5 Hz, 3.3 Hz, 2H), 7.33 (d, *J* = 7.5 Hz, 2H), 7.38 (dd, *J* = 7.8 Hz, 3.0 Hz, 2H), 7.46 (m, 2H), 7.76 (td, *J* = 7.8 Hz, 2.4 Hz, 2H), 7.86 (tt, *J* = 7.8 Hz, 1.8 Hz, 2H), 8.61 (t, *J* = 5.1 Hz, 2H, Py-H_6). ESI-MS found (calculated) for $[Cu_2(\mathbf{L^{2}*SSL^{2}*})]^{2+}$: *m/z* 350.1 (349.1); [**L^{2}*SSL^{2}*** + Cu]$^+$: *m/z*

635.1 (635.2); $[M - BF_4]^+$: *m/z* 785.1 (785.1). UV-vis in CH_3CN at 2 mM [Cu]: 260 nm (ε = 6800 M^{-1} cm^{-1}), 305 nm (ε = 3300 M^{-1} cm^{-1}).

3.6 References

1. Ording-Wenker, E. C. M.; van der Plas, M.; Siegler, M. A.; Bonnet, S.; Bickelhaupt, F. M.; Fonseca Guerra, C.; Bouwman, E., *Inorg. Chem.* **2014,** *53*, 8494-8504.
2. Thomas, A. M.; Lin, B.-L.; Wasinger, E. C.; Stack, T. D. P., *J. Am. Chem. Soc.* **2013,** *135*, 18912-18919.
3. Ording-Wenker, E. C. M.; Siegler, M. A.; Lutz, M.; Bouwman, E., *Inorg. Chem.* **2013,** *52*, 13113-13122.
4. Nielsen, M. C.; Ulven, T., *Chem. Eur. J.* **2008,** *14*, 9487-9490.
5. Addison, A. W.; Rao, T. N.; Reedijk, J.; Vanrijn, J.; Verschoor, G. C., *J. Chem. Soc., Dalton Trans.* **1984**, 1349-1356.
6. The BF_4^- anion, that is disordered over at least three orientations, shows residual electron density near the disordered components, which may indicate the presence of traces of some impurities such as Cl^-. The presence of Cl^- can be traced back to the use of chloroform in the synthesis of **L²*SSL²***. The occupancy factors of the three orientations of the disordered BF_4^- counterion and the two positions of Cl^- impurities were refined using free variables (FVAR), and their values refine to 0.382(3), 0.345(3), 0.072(3), 0.165(3), and 0.036(2) (the sum of all occupancy factors being equal to 1 for charge balance).
7. Ohta, T.; Tachiyama, T.; Yoshizawa, K.; Yamabe, T.; Uchida, T.; Kitagawa, T., *Inorg. Chem.* **2000,** *39*, 4358-4369.
8. Alvarez-Paggi, D.; Abriata, L. A.; Murgida, D. H.; Vila, A. J., *Chem. Commun.* **2013,** *49*, 5381-5383.
9. Hay, M. T.; Ang, M. C.; Gamelin, D. R.; Solomon, E. I.; Antholine, W. E.; Ralle, M.; Blackburn, N. J.; Massey, P. D.; Wang, X. T.; Kwon, A. H.; Lu, Y., *Inorg. Chem.* **1998,** *37*, 191-198.
10. Hwang, H. J.; Lu, Y., *P. Natl. Acad. Sci. USA* **2004,** *101*, 12842-12847.
11. Lukoyanov, D.; Berry, S. M.; Lu, Y.; Antholine, W. E.; Scholes, C. P., *Biophys. J.* **2002,** *82*, 2758-2766.
12. Xie, X.; Gorelsky, S. I.; Sarangi, R.; Garner, D. K.; Hwang, H. J.; Hodgsont, K. O.; Hedman, B.; Lu, Y.; Solornon, E. I., *J. Am. Chem. Soc.* **2008,** *130*, 5194-5205.
13. Barnett, S. M.; Goldberg, K. I.; Mayer, J. M., *Nature Chem.* **2012,** *4*, 498-502.
14. Sundstrom, E. J.; Yang, X.; Thoi, V. S.; Karunadasa, H. I.; Chang, C. J.; Long, J. R.; Head-Gordon, M., *J. Am. Chem. Soc.* **2012,** *134*, 5233-5242.
15. Haines, R. J.; Wittrig, R. E.; Kubiak, C. P., *Inorg. Chem.* **1994,** *33*, 4723-4728.
16. Angamuthu, R.; Byers, P.; Lutz, M.; Spek, A. L.; Bouwman, E., *Science* **2010,** *327*, 313-315.
17. Nagao, H.; Mizukawa, T.; Tanaka, K., *Inorg. Chem.* **1994,** *33*, 3415-3420.

18. Hetterscheid, D. G. H.; Smits, J. M. M.; de Bruin, B., *Organometallics* **2004,** *23*, 4236-4246.
19. Pennings, Y. C. M.; Driessen, W. L.; Reedijk, J., *Polyhedron* **1988,** *7*, 2583-2589.
20. Sheldrick, G. M., *Acta Crystallogr. Sect. A* **2008,** *64*, 112-122.
21. te Velde, G.; Bickelhaupt, F. M.; Baerends, E. J.; Guerra, C. F.; Van Gisbergen, S. J. A.; Snijders, J. G.; Ziegler, T., *J. Comput. Chem.* **2001,** *22*, 931-967.
22. http://www.scm.com/
23. Swart, M.; Ehlers, A. W.; Lammertsma, K., *Mol. Phys.* **2004,** *102*, 2467-2474.
24. Klamt, A., *J. Phys. Chem.* **1995,** *99*, 2224-2235.
25. Klamt, A.; Schuurmann, G., *J. Chem. Soc., Perkin Trans. 2* **1993**, 799-805.
26. Pye, C. C.; Ziegler, T., *Theor. Chem. Acc.* **1999,** *101*, 396-408.
27. Swart, M.; Roesler, E.; Bickelhaupt, F. M., *Eur. J. Inorg. Chem.* **2007**, 3646-3654.
28. Noodleman, L., *J. Chem. Phys.* **1981,** *74*, 5737-5743.
29. Noodleman, L.; Baerends, E. J., *J. Am. Chem. Soc.* **1984,** *106*, 2316-2327.